Int. J. Heat Mass Transfer. Vol. 31, No. 5, pp. 907–915, 1988
Printed in Great Britain

0017–9310/88 $3.00 + 0.00

Experimental and numerical investigation of natural convection in convergent vertical channels

E. M. SPARROW and R. RUIZ
Department of Mechanical Engineering, University of Minnesota, Minneapolis, MN 55455, U.S.A.

and

L. F. A. AZEVEDO
Department of Mechanical Engineering, Pontificia Universidade Catolica, Rio de Janeiro, Brazil

(*Received* 15 *July* 1987 *and in final form* 23 *October* 1987)

Abstract—Natural convection heat transfer in convergent vertical channels has been investigated both by experiments and by numerical solutions of the conservation equations. The investigation encompassed half angles of convergence between 0 (parallel-walled channel) and 15°, and the working fluid was water ($Pr \sim 5$). The channel walls were maintained at a uniform temperature which exceeded the ambient temperature, thereby giving rise to an upflow through the channel. It was found that the Nusselt numbers for the convergent channels could be brought into very close agreement with those for the parallel-walled channel by employing correlation variables based on the maximum interwall spacing as the characteristic dimension. The experimentally determined and numerically predicted Nusselt numbers were in excellent agreement, both in magnitude and with regard to all observable trends.

INTRODUCTION

THIS PAPER describes an experimental and numerical study of the buoyancy-driven fluid flow and heat transfer in a channel the walls of which converge in the flow direction. In the physical situation investigated here, the axis of the channel is vertical. The two principal walls are maintained at the same uniform temperature the value of which exceeds the temperature of the surroundings from which fluid is drawn into the channel inlet and into which fluid is discharged from the channel exit. Under these conditions, the density of the fluid in the channel is lower than that of the fluid in the surroundings. As a consequence, there is buoyancy-induced upflow in the channel. The channel inlet presents the largest cross section to the fluid flow, and the flow cross section diminishes linearly with increasing elevation.

The geometry of the flow channel is characterized by two dimensionless parameters which may be expressed in various forms. Here, the parametric description will be made via the half-angle of convergence θ and the $L/S_{\min}$ ratio, where L is the streamwise length of either principal wall and $S_{\min}$ is the minimum separation distance between the walls (i.e. at the channel exit). Half angles θ of 0, 2, 5, 10, and 15° were employed in the investigation along with $L/S_{\min}$ values of 11.4 and 22.9.

The other independent parameters are the Prandtl number and the aspect ratio, Rayleigh number product $(S/L)Ra_S$. The experiments were performed in water, and the temperature levels were set so that the mean Prandtl number was approximately five. For the computations, $Pr = 5$ was used. The $(S/L)Ra_S$ group was evaluated separately for $S = S_{\min}$, $S = S_{\text{av}}$, and $S = S_{\max}$, with different ranges and magnitudes for each. These will become apparent when the results are presented.

In the presentation of results, primary emphasis will be placed on the average Nusselt number for the channel as a whole. The first order of business is to compare the present results for $\theta = 0°$ (parallel-walled channel) with the literature. Thereafter, the convergent-channel results corresponding to the various parameters are presented. The special focus of this presentation is to seek a format which brings into congruence the results for the different degrees of convergence (i.e. for the various θ values). In particular, the ideal format is that which provides a common representation for the results for convergent and parallel-walled channels. In this regard, the correlation given in ref. [1] will be used to represent the average Nusselt number for the parallel-walled channel.

The numerical work encompassed finite-difference solutions of the governing differential equations for mass, momentum, and energy conservation in the fluid. Prior experience with the parallel-walled channel indicated that the boundary layer form of the conservation equations, when solved numerically, yielded average heat transfer results that agreed very well with those of the experiments. On this basis, the boundary layer equations are also used here for the convergent channel.

NOMENCLATURE

A	surface area of heated wall(s)
c_p	specific heat
g	acceleration of gravity
h	average heat transfer coefficient, $Q/A(T_w - T_\infty)$
k	thermal conductivity
L	streamwise length of heated wall
$\dot{m}$	mass flow rate
Nu_ξ	Nusselt number, $h\xi/k$
Pr	Prandtl number
p	static pressure
p'	reduced pressure, $p - p_\infty$
p_∞	ambient pressure
Q	heat transfer rate at channel wall(s)
Ra_ξ	Rayleigh number, $[g\beta(T_w - T_\infty)\xi^3/\nu^2]Pr$
S	spacing between channel walls
S_{av}	mean interwall spacing
S_{max}	maximum interwall spacing
S_{min}	minimum interwall spacing
T	temperature
T_b	bulk temperature
T_w	wall temperature
T_∞	ambient temperature
u, v	velocity components
u_0	inlet velocity
W	width of channel walls
x, y	Cartesian coordinates.

Greek symbols

α	thermal diffusivity
β	coefficient of thermal expansion
θ	half angle of convergence
μ	viscosity
ν	kinematic viscosity
ξ	characteristic dimension
ρ	density
ρ_∞	ambient density
ψ	stream function
ψ_w	value of ψ at channel wall
ω	transformed transverse coordinate, ψ/ψ_w.

These equations are parabolic and can be solved by a numerical scheme which incorporates unidirectional marching in the streamwise direction. The Patankar–Spalding method [2] is well suited to this computational problem. It has the special advantage of being able to handle the sloping (i.e. convergent) walls without difficulty. The numerically determined average Nusselt numbers will be compared with those determined experimentally.

To the best knowledge of the authors, there is no prior literature dealing with buoyancy-driven flow in a converging vertical channel. The parallel-walled vertical channel, which is a special case of the converging channel, has been studied extensively. Reference [1] is representative of the recent literature, and the citations listed there provide further references. All that is needed here is an accurate representation of the average Nusselt number results for the parallel-walled channel, and that is provided by ref. [1].

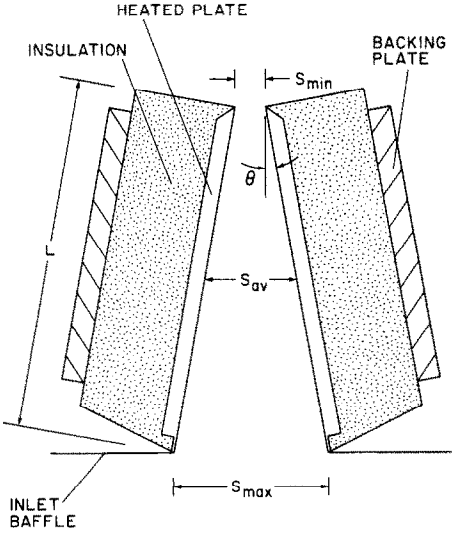

FIG. 1. Schematic diagram of the flow channel assembly used in the experimental work.

EXPERIMENTS

Flow channel

A schematic diagram of the channel assembly is presented in Fig. 1. The figure also conveys relevant geometrical nomenclature: θ, the half angle of convergence; L, the streamwise length of either principal wall; and S_{max}, S_{av}, and S_{min}, the maximum, average, and minimum interwall spacings, respectively. Note that S_{av} corresponds to the spacing at the mid-height of the channel. For concreteness, the figure illustrates one of the cases for which experiments were performed, namely, $\theta = 10°$ and $L/S_{min} = 11.4$. Subjectively speaking, the extent of the illustrated convergence appears to be significant, thereby giving perspective to the numerical values of the investigated half angles θ. The channel side walls are not shown in Fig. 1 but will be described shortly.

As seen in the figure, the channel assembly consisted of two identical principal walls, each inclined at an angle θ with respect to the vertical. Each wall was made up of a heated copper plate insulated from behind by a block of water-tolerant, closed-pore polystyrene (Styrofoam) and backed by a plexiglass plate.

Each copper plate had a streamwise length L of

14.52 cm, a width W (normal to the plane of the figure) of 9.67 cm, and a thickness of 0.635 cm. Copper was chosen for its high thermal conductivity and its relative inertness with respect to water. With regard to the latter, tarnish (i.e. oxidation) of the exposed surface of the copper plate was removed periodically between data runs with the aid of a metal polish. The upper and lower edges of the plate were contoured to avoid extraneous heat losses at those locations. A 45° bevel was cut at the upper edge while a deep, step-like recess was machined at the lower edge, leaving a residual plate thickness of 0.1 cm.

Heating was accomplished by means of electrical resistance wire installed at the rear surface of the copper plate. The wire (Teflon-coated, 0.0127-cm-diameter chromel thermocouple wire) was laid in 20 shallow spanwise (i.e. horizontal) grooves and on the tread of the leading-edge step and cemented in place with a water-resistant adhesive. The heater wires situated on the step were provided to accommodate the expected higher rates of heat transfer in the neighborhood of the leading edge. To facilitate the attainment of temperature uniformity on the front surface of the copper plate, the heating wire in the lower, middle, and upper regions of the plate was connected so as to form three separate and independently controlled circuits fed by a regulated a.c. power supply.

The adjustment of each heating circuit was guided by the readings of eight thermocouples distributed throughout the heated plate. The thermocouples were installed in holes drilled into the plate from the rear, with the junctions situated no more than 0.05 cm from the front face. Copper oxide cement was used to hold the junctions in place and to facilitate good thermal contact. The thermocouples were made from specially calibrated, Teflon-coated, 0.0254-cm-diameter chromel and constantan wire. This thermocouple pair was chosen because it provides the highest thermoelectric sensitivity of any of the commonly available thermocouples and also because it is inert in water. The thermocouple voltages were read to 1 μV.

The control afforded by the independent heating circuits enabled nearly perfect temperature uniformity to be achieved. Typically, the difference between an individual thermocouple reading and the plate mean temperature was about 1% of the plate-to-fluid temperature difference.

The rear surface of each of the heated copper plates was completely covered by a block of 3.5-cm-thick Styrofoam insulation in order to ensure that possible heat losses there would be negligible. To accommodate the special geometries at the lower and upper edges of the copper plate, the insulation actually consisted of three separate pieces. Any spaces between the plate and the insulation were carefully filled with silicone rubber sealant.

The insulation was backed by a 0.95-cm-thick plexiglass plate having streamwise and spanwise dimensions of 11.4 and 9.0 cm, respectively. The heated plate/insulation/backing plate assembly was tied together into a rigid unit by three threaded nylon rods (not shown).

The side walls of the channel consisted of a pair of vertical, parallel plates separated by a distance of 9.67 cm, which is identical to the spanwise dimension of the flow channel assembly. Each of the side walls was made from 1.27-cm-thick plexiglass. At its lower end, each side wall was rigidly attached to a horizontal baseplate also made of plexiglass. Thus, the combination of the two side walls and the baseplate was a free-standing unit into which the flow channel assembly could be inserted. Tie rods which bridged between the side walls could be tightened to hold the flow channel in place. The tie rods were situated well beyond the rear face of each of the principal walls of the channel and, therefore, did not interfere with the path of the fluid flow.

The flow channel was positioned between the side walls so that the channel inlet was situated about 12.7 cm above the baseplate. To allow fluid to enter the inlet freely from all directions, a large opening was cut in each of the side walls. The height of the opening extended all the way from the baseplate to the channel inlet. The exit of the flow channel closely coincided with the upper end of the side walls.

The experiments were performed using a common inlet configuration for all of the investigated convergent channels. As indicated in Fig. 1, the inlet cross section was framed by a *horizontal* baffle. The baffle was made of a high-strength adhesive tape which was anchored to the exposed tip of the copper plate and to the side walls.

The setting up of the flow channel between the side walls was a painstaking procedure that is described in detail in ref. [3]. The setup procedure was designed to fix the minimum separation distance S_{min}, the half angle of convergence θ, the symmetry of the respective heated plates with respect to the channel axis, the verticality of the axis, and the alignment of the lower edges of the side walls with the inlet cross section of the channel. The accuracy of the preselected S_{min} was ensured by the use of precisely machined spacer blocks, while θ was set and verified with the aid of a 0.001 in. dial-gauge-equipped caliper used to measure S_{max}.

The aforementioned setup procedure was performed with the apparatus situated outside the test chamber that was used to contain the water in which the experiments were performed. Subsequently, the apparatus was installed in the test chamber and leveled with the aid of adjustable legs that had been built into the baseplate.

Fluid environment

The experiments were carried out in a thermally guarded test chamber filled with distilled water. The test chamber dimensions were chosen sufficiently large to provide a fluid environment that would appear to

be infinite with respect to processes occurring in the flow channel. Thermal guarding was achieved by a tank-in-tank arrangement, whereby the test chamber was surrounded by a still larger chamber. Distilled water was also used to fill the inter-chamber space, in which was situated a temperature control and water circulation unit.

Both chambers were fabricated from 1.27-cm-thick plexiglass. The respective dimensions of the inner and outer chambers were $74 \times 43 \times 44$ cm and $102 \times 66 \times 48$ cm (length × width × height). Heat and moisture losses from the free surfaces of the water in the test chamber and in the inter-chamber space were suppressed by a coated sheet of Styrofoam insulation lined with a plastic vapor barrier.

The experimental apparatus was positioned centrally with respect to the length, width, and height of the test chamber. As a result of this positioning, the exit cross section of the flow channel was situated at least 12.7 cm beneath the free surface of the water. Similarly, as noted earlier, the channel inlet was about 12.7 cm above the baseplate of the apparatus.

A vertical array of three chromel–constantan thermocouples supported by a plexiglass rod was used to measure the temperature of the water in the test chamber. The three thermocouples were respectively positioned 7.6, 16.5, and 24.1 cm above the floor of the chamber. The array was situated about 12 cm to the side of the flow channel—well away from the direct line of any fluid flow induced by the presence of the channel.

In addition to the thermocouples, an ASTM-certified thermometer with a smallest scale division of 0.1°F was installed in the test chamber and in the inter-chamber space. These two thermometers were placed close to each other, separated only by the plexiglass wall of the test chamber. A precondition for the initiation of a data run (i.e. prior to the initiation of heating at the channel walls) was that (1) the two thermometers displayed identical readings, (2) the readings of the three thermocouples in the test chamber were the same, and (3) the temperatures indicated by the thermocouples and the thermometers were equal. The fulfillment of these requirements guaranteed the absence of extraneous natural convection currents in the test chamber prior to the initiation of a data run. The steps performed to achieve the desired temperature uniformity are described in ref. [3].

A data run was initiated by applying power to the heating circuits embedded in the walls of the flow passage. The individual voltages applied to each circuit to obtain isothermal-wall boundary conditions had been set in advance on the basis of information from prior runs. Steady-state conditions were achieved within 15 min or less after the initiation of a run, at which point data were collected. Temperature stratification in the test chamber due to the heating of the flow channel walls was negligible. The largest temperature variation among the vertical array of thermocouples never exceeded 1% of the plate-to-fluid temperature difference.

DATA REDUCTION

The objective of the data reduction procedure was to evaluate Nusselt and Rayleigh numbers from the measured temperatures and heat transfer rates. These quantities are defined here as

$$Nu_\xi = h\xi/k, \quad h = Q/A(T_w - T_\infty) \tag{1}$$

$$Ra_\xi = [g\beta(T_w - T_\infty)\xi^3/\nu^2]Pr. \tag{2}$$

In these equations, ξ represents an assignable characteristic dimension. Here, three readily identifiable choices for ξ will be considered, namely, S_{min}, S_{av}, and S_{max}, with a view to finding a relationship between Nu and Ra which is independent of θ and of a characteristic dimension ratio (e.g. L/S_{min}).

In evaluating the average heat transfer coefficient h, two possibilities presented themselves. One was to determine h separately for each of the two heated walls of the channel and then to average the individual values. The other approach was to find h directly for the two-plate system. The two methods yielded virtually indistinguishable results, thereby testifying to the geometrical and thermal symmetry of the experimental setup and its operation. For concreteness, the second method will be described here.

The temperature T_w of the exposed surfaces of the heated walls was obtained by averaging over all 16 thermocouples embedded in the two walls, while T_∞ was the average of the three thermocouples in the fluid environment. As noted earlier, the nonuniformities in both the wall and fluid temperatures were negligible. The heat transfer rate Q was the sum of the electric power inputs to the six heating circuits of the channel (three per heated wall), since extraneous heat losses were shown to be negligible in ref. [3]. Corresponding to Q, the area A appearing in equation (1) is equal to the exposed surface area of both the heated walls, i.e. $2LW$.

The thermophysical properties were evaluated at a reference temperature $(T_w + T_\infty)/2$. Algebraic descriptions of k, ρ, μ, and c_p for liquid water are presented in ref. [3], and β was obtained by differentiation of the equation for ρ. The Prandtl number Pr and kinematic viscosity ν appearing in equation (2) were obtained by substituting the aforementioned property values into $c_p\mu/k$ and μ/ρ, respectively.

NUMERICAL SOLUTIONS

The numerical work will be performed for laminar flow and for fluid properties that are constant except for the density variation which contributes to the buoyancy force. The initial formulation of the problem is made in x, y Cartesian coordinates, where the x coordinate is vertical and the y coordinate is horizontal. In particular, x is measured vertically upward along the symmetry axis of the flow channel, with

$x = 0$ in the cross section of the channel inlet. The y axis lies in the inlet cross section; $y = 0$ at the symmetry line.

In the analysis of buoyant flows in open-ended channels that are situated in an isothermal fluid environment (temperature T_∞), it is usual to introduce a reduced pressure p' as

$$p'(x) = p(x) - p_\infty(x) \tag{3}$$

where $\mathrm{d}p_\infty/\mathrm{d}x = -\rho_\infty g$. With this, and with the Boussinesq density–temperature relation ($\Delta\rho = -\beta\rho\Delta T$), the x-momentum equation can be written as

$$u(\partial u/\partial x) + v(\partial u/\partial y) = -(1/\rho)(\mathrm{d}p'/\mathrm{d}x) + g\beta(T - T_\infty) + \nu(\partial^2 u/\partial y^2). \tag{4}$$

The mass conservation and energy equations are used in their conventional forms, i.e.

$$\partial u/\partial x + \partial v/\partial y = 0 \tag{5}$$

$$u(\partial T/\partial x) + v(\partial T/\partial y) = \alpha(\partial^2 T/\partial y^2). \tag{6}$$

As noted in the Introduction, the problem was solved numerically by making use of the Patankar–Spalding method [2]. That method is based on a transformed form of the conservation equations in which the independent variables are x, ω rather than x, y. The ω coordinate is defined as

$$\omega = \psi/\psi_w \tag{7}$$

where ψ is the stream function

$$\rho u = \partial\psi/\partial y, \quad \rho v = -\partial\psi/\partial x$$

with ρ = constant in the present problem. The stream function may be assigned a value of zero along the symmetry axis of the channel. In addition, ψ_w is the rate of mass flow passing through the cross section of the channel between the symmetry axis and one of the walls. Since the walls are impermeable, ψ_w is a constant.

If the solution domain is taken to be the portion of the channel between the axis and the right-hand wall, then in the x, ω coordinates the domain is a rectangle defined by

$$0 \leqslant \omega \leqslant 1, \quad 0 \leqslant x \leqslant L\cos\theta. \tag{8}$$

This solution domain was spanned by a uniform grid consisting of 600 points in the x direction and 82 points in the ω direction.

The Patankar–Spalding method is a marching scheme. The marching begins at $x = 0$ and proceeds along the channel to $x = L\cos\theta$. To take account of the convergence of the channel, the cross-sectional area of the channel between the axis and the wall at each x station visited during the marching procedure is provided as input to the computer program. This information is used in conjunction with mass conservation to determine the axial pressure distribution.

The boundary conditions required by the Patankar–Spalding method include the specification of velocity and thermal information at the channel inlet, at the axis, and at the channel wall. The scheme has no need for boundary conditions for the pressure and cannot make direct use of such information were it to be provided.

The boundary condition information that is available for the present problem does not completely match with the needed information that was noted in the preceding paragraph. Whereas velocity boundary conditions are available at the wall (zero normal and tangential components) and at the axis (symmetry conditions), the velocity field is unknown at the inlet. For the temperature, the boundary conditions are available at the inlet ($T = T_\infty$), at the wall ($T = T_w$), and at the axis (symmetry condition), as needed by the numerical scheme.

In compensation for the aforementioned deficit in velocity boundary condition information, there is information about the pressure. At the inlet, the static pressure is somewhat lower than the ambient pressure at the same elevation due to the acceleration of the flow from zero velocity in the ambient to the inlet velocity u_0 (assumed axial and uniform). It will be assumed that this pressure drop is $\rho u_0^2/2$, so that

$$p' = -\rho u_0^2/2 \tag{9}$$

at $x = 0$. Furthermore, at the exit, if the flow discharges in a jet-like manner without pressure recovery

$$p' = 0 \tag{10}$$

at $x = L\cos\theta$.

The use of the pressure information conveyed by equations (9) and (10) will now be described. For a given physical situation defined by geometric and thermal parameters to be identified shortly, a value of the axial velocity u_0 at the inlet is guessed. (u_0 is assumed uniform and the transverse velocity is assumed zero.) This information enables the marching procedure to be executed, yielding the velocity and temperature fields throughout the solution domain. Also, with the value of p' at $x = 0$ from equation (9), the solution yields $p'(x)$ and, in particular, the value of p' at $x = L\cos\theta$. If that value of p' is not zero, as required by equation (10), a new numerical value of u_0 is assigned and the problem is solved again. This procedure is continued until a value of u_0 is found which satisfies equation (10). Convergence of the procedure was hastened by the use of the Newton–Raphson technique.

The parameters used to define each physical situation include the half angle θ, the dimension ratio $L/S_{\min}$, the Rayleigh number $Ra_{S_{\min}}$, and the Prandtl number Pr. The latter was set equal to 5 for all the computations in order to reflect the operating temperatures of the experiments. The values of the other parameters were varied to cover the ranges encountered during the experimental work.

To provide results which enable comparisons with the experimental data, primary attention was given to the average Nusselt numbers predicted by the numeri-

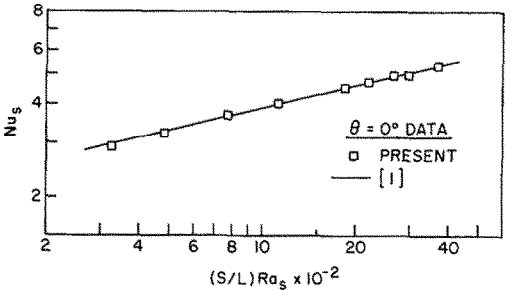

FIG. 2. Nusselt number results for the parallel-walled channel, $L/S = 22.9$.

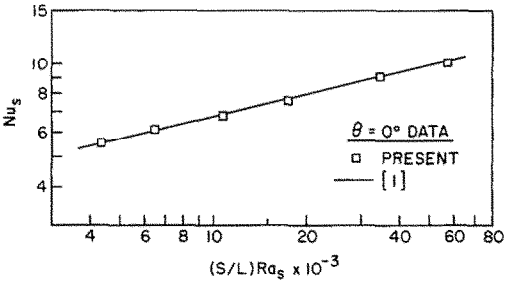

FIG. 3. Nusselt number results for the parallel-walled channel, $L/S = 11.4$.

cal solutions. To this end, the overall rate of heat transfer Q was obtained from

$$Q = \dot{m}c_p(T_{b,out} - T_{b,in}). \quad (11)$$

Since the solution domain encompasses only half the channel, the Q value given by equation (11) corresponds to heat transfer at one of the channel walls. Similarly, the mass flow rate $\dot{m}$ is given by $\rho u_0 S_{max}/2$. The quantities $T_{b,out}$ and $T_{b,in}$ are, respectively, the exit and inlet bulk temperatures, the latter being equal to T_∞.

The Q values obtained from equation (11) were introduced into equation (1) to yield heat transfer coefficients and Nusselt numbers. Note that for the evaluation of h, the area A is now that of one of the heated walls. The numerically predicted Nusselt numbers will be compared with the experimental data shortly.

As a final remark about the numerical work, it may be noted that the Patankar–Spalding method contains approximations which are based on small wall slopes. Because of this, it was deemed inadvisable to perform calculations for θ values larger than 15°.

RESULTS AND DISCUSSION

Parallel-walled channel

The first set of results to be presented pertains to the parallel-walled channel, which corresponds to $\theta = 0°$. These data were obtained to serve as a baseline against which to compare the convergent-channel results. For the parallel-walled channel, the uniform separation distance between the walls, to be donated by S, will be used as the characteristic dimension in the Nusselt and Rayleigh numbers defined by equations (1) and (2) (i.e. ξ is to be replaced by S).

The parallel-channel Nusselt numbers Nu_S for the $L/S = 22.9$ and 11.4 aspect-ratio channels are presented in Figs. 2 and 3, respectively. The abscissa variable $(S/L)Ra_S$ is a composite parameter which has been used successfully in the past (e.g. ref. [1]) to correlate the dependence of the Nusselt number on both L/S and Ra_S for parallel-walled channels.

In addition to the data, each figure contains a solid line the equation of which is

$$Nu_S = 0.740[(S/L)Ra_S]^{0.240}. \quad (12)$$

This equation represents the least-squares correlation of the experimental data of ref. [1] for water ($Pr \cong 5$), which covered the range of $(S/L)Ra_S$ from 2×10^2 to 1.5×10^5. To lend support to equation (12), numerical solutions for the parallel-walled channel were carried out using the scheme described in the preceding section of the paper. The solutions were performed for the $(S/L)Ra_S$ range of Figs. 2 and 3. The numerically determined Nusselt numbers were compared with those of equation (12), with agreement in the 1–2% range.

It may also be noted that the 0.240 exponent in equation (12) is very close to the $\frac{1}{4}$-power exponent which typifies laminar natural convection. A $\frac{1}{4}$-power correlation, also presented in ref. [1], was not quite as good a representation of the data of ref. [1] as is equation (12).

Examination of Figs. 2 and 3 reveals excellent agreement between the present data and the correlating line from ref. [1]. Typically, the deviations between the data and the line are in the 1–2% range. This level of agreement is reassuring. The flow channel used in the present experiments made use of the same heated plates that were used in ref. [1], but the remaining components of the channel were different. The fact that the Nusselt numbers remained the same for the two versions of the flow channel offers testimony about the generality of the results. In the subsequent presentation of convergent-channel results, equation (12) will be used to represent the present parallel-channel data.

S_{min}-Based presentation variables

As noted in the Introduction, the convergent-channel Nusselt number results will be presented using several candidate characteristic dimensions (S_{min}, S_{av}, and S_{max}). The objective of this approach is to find a correlation format which merges the convergent-channel results with those for the parallel-walled channel.

The first presentation of the convergent-channel results is based on S_{min} as the characteristic dimension. The Nusselt number results for the $L/S_{min} = 22.9$ and 11.4 aspect-ratio channels are respectively presented

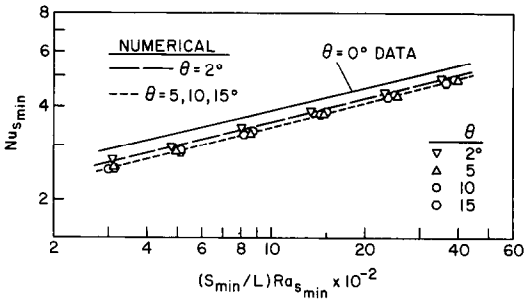

FIG. 4. S_{min}-Based Nusselt number presentation, $L/S_{min} = 22.9$.

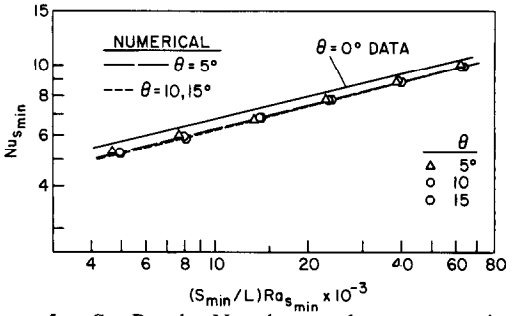

FIG. 5. S_{min}-Based Nusselt number presentation, $L/S_{min} = 11.4$.

in Figs. 4 and 5. As seen from the figures, the form of the abscissa variable resembles that used for the parallel-walled channel. Since the numerical values of this variable did not overlap for the two investigated aspect ratios, it was deemed appropriate to present each aspect ratio in a separate figure.

In each figure, in addition to the experimental data points corresponding to half angles θ of 2, 5, 10, and 15°, the parallel-channel data ($\theta = 0°$) are conveyed by a solid line representing equation (12). The predictions of the numerical solutions are represented by the long-dash and short-dash lines.

From an examination of Fig. 4, it is seen that the data corresponding to $\theta = 5$, 10, and 15° cluster together, so that in this range the Nusselt number is independent of θ. These data fall in a band which is about 15% below the parallel-channel results at the lower end of the abscissa range and 10% below at the upper end of the range. Thus, in the range between $\theta = 0$ and 5°, the Nusselt number varies with θ by 10–15%. The nature of this variation was investigated by collecting data at $\theta = 2°$. The 2° data fell 6–8% below that for the parallel-walled channel. Thus, the sensitivity of the Nusselt number to θ is primarily confined to small θ values.

Figure 4 also indicates that the deviations of the convergent-channel data from the parallel-channel data tend to decrease with increasing values of the abscissa variable. This trend is reinforced in Fig. 5, where the values of the abscissa variable are about an order of magnitude larger than those of Fig. 4. In Fig. 5, the $\theta = 10$ and 15° data are virtually coincident and fall 5–10% below those for $\theta = 0°$, with the largest deviations at the lower end of the abscissa and the smallest deviations at the upper end.

The $\theta = 5°$ data display a slight scatter, tending to deviate from the 10 and 15° data at some abscissa values and to coincide at others. Overall, the 5° data fall 4–6% below the parallel-channel results. Because of the diminished sensitivity of the Nusselt number to θ for the conditions of Fig. 5, no $\theta = 2°$ data were collected for the $L/S_{min} = 11.4$ aspect ratio.

In physical terms, the message of Figs. 4 and 5 is that the heat transfer coefficient for a convergent channel with a minimum interwall spacing S_{min} is lower than that for a parallel-walled channel the interwall spacing of which is equal to S_{min}. The maximum decrease in the heat transfer coefficient encountered here is about 15%. Another significant message is that the use of S_{min} as the characteristic dimension does not fulfill the objective of merging the convergent-channel results with those for the parallel-walled channel.

Attention will now be turned to the comparison in Figs. 4 and 5 of the numerically predicted and experimentally determined Nusselt numbers. Inspection of these figures shows that truly excellent agreement prevails. Not only do the lines representing the numerical results pass through the data, but also, all of the trends in the data are corroborated. In particular, in Fig. 4, the independence of the Nusselt number from θ for $\theta = 5$, 10, and 15°, earlier identified in the experimental data, is also a characteristic of the numerical results. A similar finding applies for the $\theta = 10$ and 15° results in Fig. 5.

The outstanding agreement between the experimental and numerical results lends support to both the experimental technique and to the computational model. Although the comparison between the experimental and numerical results was made in the presentation format based on S_{min} as the characteristic dimension, an identical outcome would be forthcoming in presentation formats based on S_{av} and S_{max}. Therefore, no further comparisons need be made.

S_{av}-Based presentation variables

The results will now be presented in a format in which S_{av} is used as the characteristic dimension, and Fig. 6 has been prepared for this purpose. The abscissa variable used in the figure resembles that for the parallel-walled channel but with S replaced by S_{av}. In terms of this abscissa variable, the data for the two investigated aspect ratios overlap and, because of this, the two aspect ratios are brought together on a single figure. To accommodate the four-decade range of the abscissa variable, both upper and lower scales are used. The closed and open data symbols respectively denote the $L/S_{min} = 11.4$ and 22.9 aspect ratios.

The data for the parallel-walled channel are represented by the solid line, which is a plot of equation (12). Since the abscissa range of Fig. 6 extends beyond that of the data on which equation (12) was based,

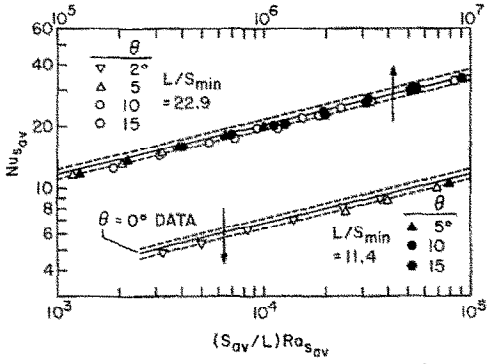

FIG. 6. S_{av}-Based Nusselt number presentation.

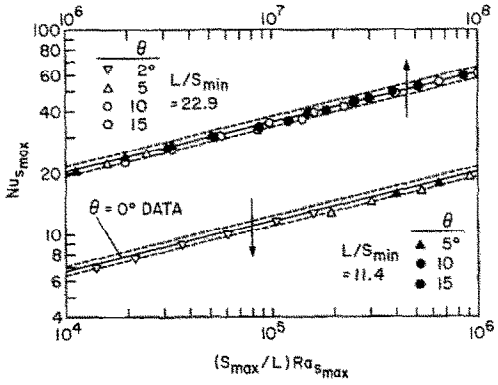

FIG. 7. S_{max}-Based Nusselt number presentation.

the solid line is, in part, an extrapolation. The dashed lines bound a $\pm 5\%$ band around the parallel-channel results.

An overview of Fig. 6 indicates that the use of S_{av} as the characteristic length brings the convergent-channel and parallel-channel Nusselt numbers closer together than did the use of S_{min}. In particular, in Fig. 6, the majority of the convergent-channel data fall within 5% of the parallel-channel line, with the greatest deviation being 9%. Virtually all of the data fall below the line, which continues the behavior which occurred in the S_{min} presentation format, where all of the data fell below the line. Within any set of data characterized by fixed L/S_{min} and θ, it may be observed in Fig. 6 that the deviations between the data and the line decrease with increasing values of the abscissa variable, a trend also encountered in the S_{min} format.

In addition to the weakened dependence of the Nusselt number on θ evidenced in Fig. 6, the figure also shows that the data are insensitive to the aspect ratio (i.e. the open and closed symbols appear to belong to a single set of data). This capability of the abscissa variable to bring together the different aspect ratios is similar to what has been found for the parallel-walled channel.

The physical message of Fig. 6 is that for a convergent channel with a mean interwall spacing S_{av}, the heat transfer coefficient will be slightly below that for a parallel-walled channel with spacing $S = S_{av}$.

S_{max}-Based presentation variables

The final presentation of the Nusselt number results, based on S_{max} as the characteristic dimension, is made in Fig. 7. This figure is identical in format to Fig. 6, except that S_{av} has been replaced by S_{max}. By carefully inspecting and comparing Figs. 6 and 7, it is readily seen that the S_{max} presentation format yields the least deviations between the convergent-channel and parallel-channel Nusselt numbers.

In the S_{max} format, virtually all of the convergent-channel data fall within 5% of the parallel-channel line, and nearly half of the data are within 2% of the line. Furthermore, although the majority of the data continue to fall below the line, there are numerous data points which lie squarely on it or fall slightly above it.

These observations suggest that equation (12) can be generalized as applicable to both convergent and parallel-walled channels. The generalized equation follows as

$$Nu_{S_{max}} = 0.740[(S_{max}/L)Ra_{S_{max}}]^{0.240}. \qquad (13)$$

Based on the present results, equation (13) should be valid at least for half angles θ between 0 and 15°.

According to Fig. 7 and equation (13), the heat transfer coefficients for a convergent channel with a maximum interwall spacing of S_{max} are, for practical purposes, equal to those for a parallel-walled channel with interwall spacing $S = S_{max}$.

CONCLUDING REMARKS

Complementary experimental and numerical studies have been performed to investigate natural convection heat transfer in a convergent vertical channel. The channel walls were maintained at a uniform temperature which exceeded the ambient temperature, thereby giving rise to an upflow through the channel. Both the experimental and numerical work were carried out for half angles of convergence in the range from 0 (parallel-walled channel) to 15° and for two channel aspect ratios (streamwise length of channel wall to typical cross-section dimension). For each channel configuration, the Rayleigh number was varied by a factor of 13–14 by varying the wall-to-ambient temperature difference. The working fluid for the experiments was water with a nominal Prandtl number of 5, and the numerical solutions corresponded to this Prandtl number value.

Primary attention was focused on the average heat transfer coefficient and Nusselt number. The main objective of the presentation of results was to find a correlation format which merged the convergent-channel Nusselt number results with those for the parallel-walled channel. In this regard, three candidate characteristic dimensions were considered,

namely, S_{min}, S_{av}, and S_{max}, respectively the minimum, mean, and maximum spacing between the channel walls.

It was found that the merging was best accomplished by the use of S_{max} as the characteristic dimension. In terms of correlation variables involving S_{max}, deviations between the convergent-channel and parallel-channel Nusselt numbers were limited to about 5%. The universal Nusselt number correlation applicable to both types of channels is conveyed by equation (13).

The experimentally determined and numerically predicted Nusselt numbers were in excellent agreement, not only in magnitude but also with regard to all observable trends.

REFERENCES

1. L. F. A. Azevedo and E. M. Sparrow, Natural convection in open-ended inclined channels, *J. Heat Transfer* **107**, 893–901 (1985).
2. S. V. Patankar and D. B. Spalding, *Heat and Mass Transfer in Boundary Layers*, 2nd Edn. Intertext Books, London (1970).
3. R. Ruiz, Natural convection heat transfer in partially enclosed configurations, Ph.D. thesis, Department of Mechanical Engineering, University of Minnesota, Minneapolis, Minnesota (1986).

ETUDE EXPERIMENTALE ET NUMERIQUE DE LA CONVECTION NATURELLE DANS DES CANAUX CONVERGENTS VERTICAUX

Résumé—On étudie la convection naturelle thermique dans des canaux convergents verticaux, à la fois expérimentalement et par résolution numérique des équations de conservation. On considère des demi-angles de convergence entre 0 (canal à parois parallèles) et 15°, le fluide de travail étant l'eau ($Pr \sim 5$). Les parois du canal sont maintenues à une température uniforme qui dépasse la température ambiante, ce qui cause l'élévation du fluide dans le canal. On trouve que le nombre de Nusselt dans les canaux convergents peuvent être ramenés à un accord serré avec celui du canal à parois parallèles en employant des variables basées sur la distance maximale entre paroi comme dimension caractéristique. Les nombres de Nusselt déterminés expérimentalement et par le calcul sont en excellent accord, à la fois en grandeur et en tendances observables.

EXPERIMENTELLE UND NUMERISCHE UNTERSCHUNG DER NATÜRLICHEN KONVEKTION IN KONVERGENTEN SENKRECHTEN KANÄLEN

Zusammenfassung—Der Wärmeübergang bei natürlicher Konvektion in konvergenten senkrechten Kanälen wurde experimentell und mit Hilfe numerischer Lösungen der Bilanzgleichungen untersucht. Der halbe Konvergenzwinkel betrug zwischen 0° (parallele Wände) und 15°, das Arbeitsfluid war Wasser ($Pr \sim 5$). Die Kanalwände wurden auf konstanter Temperatur (oberhalb der Umgebungstemperatur) gehalten, so daß sich eine Aufwärtsströmung einstellte. Es wurde festgestellt, daß die Nusselt-Zahlen bei konvergenten Kanälen sehr gut mit denen bei parallelen Wänden übereinstimmten, wenn Variablen zur Umrechnung herangezogen werden, die mit der maximalen Kanalbreite als charakteristischer Länge gebildet werden. Experimentell bestimmte und numerisch berechnete Nusselt-Zahlen stimmten sehr gut überein, sowohl bezüglich der Größe als auch bezüglich aller beobachteter Trends.

ЭКСПЕРИМЕНТАЛЬНОЕ И ЧИСЛЕННОЕ ИССЛЕДОВАНИЕ ЕСТЕСТВЕННОЙ КОНВЕКЦИИ В СУЖАЮЩИХСЯ ВЕРТИКАЛЬНЫХ КАНАЛАХ

Аннотация—Выполнено экспериментальное исследование естественноконвективного теплопереноса в сужающихся вертикальных каналах и численное интегрирование соответствующих уравнений сохранения. Рассматривалась половина углов сужения от 0 (канал с параллельными стенками) до 15°; в качестве рабочей жидкости использовалась вода ($Pr \sim 5$). Температура стенок канала поддерживалась постоянной, превышающей температуру окружающей среды, что приводило к возникновению восходящего потока в канале. Найдено, что числа Нуссельта для сужающихся каналов могут быть приведены в хорошее соответствие с числами Nu для канада с параллельными стенками с помощью обобщенных переменных, использующих в качестве характерного размера максимальное расстояние между стенками. Экспериментально определенные и численно рассчитанные числа Нуссельта находились в хорошем соответствии.